Threonine phosphorylation regulates the molecular assembly and signaling of EGFR in cooperation with membrane lipids

Ryo Maeda[1], Hiroko Tamagaki-Asahina[2], Takeshi Sato[2], Masataka Yanagawa[1], and Yasushi Sako[1,3,*]

[1]Cellular Informatics Laboratory, RIKEN CPR, Wako, Saitama 351-0198, Japan; [2]Kyoto Pharmaceutical University, 5, Misasagi-cho, Yamashina, Kyoto, 607-8414, Japan; [3]CREST JST, 4-1-8, Honcho, Kawaguchi, 332-0012, Japan

*To whom correspondence should be addressed. E-mail: sako@riken.jp

Abstract

The cytoplasmic domain of the receptor tyrosine kinases (RTKs) plays roles as a phosphorylation enzyme and a protein scaffold but the regulation of these two functions is not fully understood. We here analyzed assembly of the transmembrane (TM)-juxtamembrane (JM) region of EGFR, one of the best studied species of RTKs, by combining single-pair FRET imaging and a nanodisc technique. The JM domain of EGFR contains a threonine residue that is phosphorylated after ligand association. We observed that the TM-JM peptides of EGFR form anionic lipid-induced dimers and cholesterol-induced oligomers. The two forms involve distinct molecular interactions, with a bias towards oligomer formation upon threonine phosphorylation. We further analyzed the functions of whole EGFR molecules, with or without a threonine to alanine substitution in the JM domain, in living cells. The results suggested an autoregulatory mechanism in which threonine phosphorylation of the JM domain causes a switch from kinase activation dimers to scaffolding oligomers.

Introduction

Epidermal growth factor receptor (EGFR) is an RTK responsible for cell proliferation and differentiation (1, 2) and consists of five domains; an extracellular domain that interacts with extracellular ligands, a single-pass transmembrane (TM) helix, a juxtamembrane (JM) domain, a cytoplasmic kinase domain, and a C-terminal tail domain for interaction with various cytoplasmic proteins (3, 4). Ligand association changes the conformation of EGFR in its extracellular domain (5) and induces formation of an asymmetric dimer of the intracellular kinase domains (6). This dimerization subsequently results in the phosphorylation of tyrosine residues on the tail domain and the recruitment of intracellular signal proteins such as GRB2 and PLCγ containing SH2 and/or PTB domains (7). Although the atomic structures of most of the EGFR domains excluding the tail domain have been elucidated individually (5, 6, 8-10), the overall architecture of this protein has not yet been revealed, leaving several unanswered questions about the molecular mechanisms underlying its functions. The correlation between the arrangement of EGFR molecules and their function is therefore still controversial, e.g., it has long been established that the dimerization of EGFR is necessary and sufficient for kinase activation (11), whereas several studies have reported the importance of higher-order oligomerization for EGFR-mediated signal transduction (12-14).

The TM helix and the JM domain (TM-JM) of EGFR play important roles in the conformational coupling of ligand binding to its activation and oligomerization (9, 11, 15). Previous NMR studies and molecular dynamics simulations have suggested that the TM domain forms an α-helix dimer that undergoes a change in the interaction between GXXXG motives (9, 16, 17) following the ligand association with its extracellular domains (17, 18). This information regarding conformational changes in the TM dimer is then transmitted to the JM domain which comprises a JM-A (N-terminal half) region that can form an antiparallel helix dimer, and a JM-B (C-terminal half) region which makes intramolecular contact with the kinase domain (11). Both these JM regions contribute to the stable formation of an asymmetric kinase dimer conformation, which is crucial for kinase activation. The JM-A domain is rich in Lys and Arg residues, several of which are thought to interact with anionic lipid molecules of the plasma membrane and promote antiparallel dimer formation (19-21). In addition to the phospholipid species, cholesterol is a major component of the plasma membrane, mainly distributed as lipid rafts and caveolae, and has been implicated in the regulation of membrane fluidity and receptor function. Previous studies have shown that EGFR molecules are clustered in lipid rafts (14, 22), suggesting an interaction with cholesterols. Of note in this regard, it has been reported that the depletion of cholesterols induces various effects on EGFR signaling,

66 also this remains controversial (23-25). Another important factor in the regulation of
67 EGFR through the TM-JM is the phosphorylation of Thr654 at the JM-A domain.
68 Although Thr phosphorylation is known to be involved in EGFR deactivation, the precise
69 mechanism of this is still elusive (26).
70 In our present study, by combining single-pair FRET measurements and
71 nanodisc technology, we studied how the functions of anionic lipids, cholesterols, and
72 EGFR Thr654 phosphorylation (pT654) are orchestrated to achieve the regulation of
73 dimerization and/or oligomerization of EGFR. We previously reported that anionic lipids
74 cause the dimerization of JM domains, and that pT654 together with acidic lipids induces
75 the dissociation of the EGFR dimer (20). In this current study, we report that both the TM
76 and JM protomers of EGFR are positioned closer to each other in the presence of
77 cholesterols than in the EGFR dimers promoted by anionic lipids. Furthermore, we found
78 that TM-JM peptides were oligomerized in cholesterol containing membranes, which was
79 promoted by pT654. Finally, in living cells expressing whole EGFR molecules, we
80 observed differential functional roles of this crucial signaling factor that are dependent on
81 the pT654 levels. Our results suggest that the membrane cholesterol and pT654
82 cooperatively shift the EGFR function from the kinase dimer to the scaffold oligomer.
83

Results

Incorporation of TM-JM peptides into nanodiscs

Synthesized peptides of the TM-JM region of EGFR were prepared and labeled with a fluorophore Cy3 or Cy5 at the N-terminus (TM terminal region) or C-terminus (JM terminal region), respectively (Fig. 1a). The peptides were reconstituted into nanodisc structures with membrane scaffold proteins (MSPs) and lipid molecules (Fig. 1b, c). Mixtures of POPC (PC), POPS (PS), and cholesterol were used for reconstruction (Fig. 1d). The nanodiscs containing cholesterol showed two peaks following size exclusion gel chromatography, one of which had a smaller disc size relative to that without cholesterol (Fig. 1e). To avoid the effects of disc size, we collected and used nanodiscs involved in the first peak fraction which had a similar size without cholesterol. This fraction was composed of the same ratio of lipids as used in the preparation (Fig. 1f). Synthesized TM-JM peptides with pT654 were also reconstituted into nanodiscs. The nanodisc construction was examined under a transmission electron microscope (Fig. 1g). In total, 16 types of nanodiscs were applied to subsequent single-molecule measurements. Fractions of PS (inner leaflet) and cholesterol (inner and outer leaflets) mimicked those in the plasma membrane.

TM-TM interaction in the EGFR dimer

Nanodiscs containing Cy3 and Cy5-labeled peptides were immobilized onto glass surfaces and illuminated with a 532-nm laser for Cy3 excitation. A portion of the fluorescent spots contained Cy5 fluorescence derived from the occurrence of FRET (Fig. 2a, b). Based on the fluorescence intensity, we selected nanodiscs containing one Cy3- and one Cy5-labeled peptide and calculated the FRET efficiency, E_{FRET} (Fig. 2c).

We first examined the interactions between the N-terminal regions of the TM domains (Fig. 3). When Thr654 was not phosphorylated and the membrane contained only PC as lipid species, E_{FRET} distributed with a peak at a relatively high (> 0.90; Table I) value (Fig. 3a), indicating close proximity of the two TM domains. There may be additional stable structures between the TM domains, as suggested by the small peaks and shoulders in the E_{FRET} distribution. The addition of anionic lipid PS caused few effects, i.e., the TM dimers were maintained as the major structure (Fig. 3b). Peptides with pT654 slightly decreased the major peak positions of the E_{FRET} distributions in the PC or PC/PS membranes (Fig. 3e, f). The smooth distribution of the pT654 peptides suggested that pThr654 had homogenized possible substructures of the TM dimers of non-phosphorylated peptides. PS had a little effect on the TM-TM interactions regardless of the Thr654 phosphorylation. The presence of cholesterol in the membrane concentrated

120 the distributions to a high E_{FRET} (> 0.95) region (Fig. 3c, g, h), indicating that the N-
121 terminal regions of TM-TM dimers were positioned in extremely close proximity.
122 Although the peak position was similar in PC and PC/cholesterol membranes (Fig 3a, c;
123 Table I), the distribution in PC/cholesterol membrane was more accumulated at the peak
124 position. It also should be noted that the accumulation at a high E_{FRET} region was a
125 remarkable observation for pT654 peptides. Thus, pT654 and the presence of membrane
126 cholesterol decreased the distance between the two N-termini of the TM domains in
127 cooperation. PS competed with cholesterol when Thr654 was non-phosphorylated (Fig.
128 3d).
129
130 **JM-JM interaction in the EGFR dimer**
131 To examine the effects of lipid species and pT654 on JM-JM interaction, E_{FRET}
132 distributions were determined under the C-terminus labeling (Fig. 4). In PC membrane,
133 E_{FRET} was broadly distributed with a peak around 0.81 (Fig. 4a; Table I). It is plausible
134 that the JM-A dimers are fluctuating between minor dissociation and major association
135 states. In the PC/PS membrane, the peak fraction was increased, indicating that PS
136 stabilized the JM-A dimer conformation (Fig. 4b). pThr654 increased the low FRET
137 fraction in the PC/PS membrane (Fig. 4f) but showed little effect in the PC membrane
138 (Fig. 4e). These results confirmed the results of our previous study (20). Cholesterol
139 moved the E_{FRET} peak between non-phosphorylated peptides to higher values (0.93–0.94)
140 regardless of whether it was a PC or PC/PS membrane (Fig. 4c, d), i.e., cholesterol forced
141 the C-termini of the JM-A domains to position closer.
142 The mixed effects of cholesterol and pT654 on the JM-JM interaction were
143 further examined. In the PC membrane (Fig. 4g), cholesterol increased the high FRET
144 population to a comparable level to those shown for non-phosphorylated peptides.
145 Cholesterol in the PC/PS membrane (Fig. 4h) reversed the E_{FRET} distribution seen in the
146 PC/PS membrane without cholesterol (Fig. 4f) to that observed in the PC membrane (Fig.
147 4e) i.e. minor low FRET and major high FRET states in the PC/PS/cholesterol membrane.
148 However, it should be noted that the E_{FRET} values were not as large as those found in other
149 conditions with cholesterol (Fig. 4c, d, g), i.e., the cholesterol effect on JM-JM interaction
150 was partially diminished by the coexistence of PS and pThr654. Overall, our data showed
151 that cholesterol increased the proximity between the C-terminus of JM domains in PC
152 and PC/PS membranes, and that this effect overrode that of pThr654 in the PC/PS
153 membrane.
154
155 **Higher-order oligomerization of TM-JM peptides**

156 We speculated that the accumulation of EGFR in lipid rafts, which has been reported in
157 previous studies, could be an effect of cholesterol in the raft membrane. We examined the
158 assembly of TM-JM peptides in the nanodiscs, collecting images of fluorescent spots
159 containing only Cy3-labeled peptides to avoid interference from the effects of FRET
160 occurring between Cy3 and Cy5. Figure 5 displays the fluorescence intensity histograms
161 of C-terminus-labeled TM-JM peptides in nanodiscs containing or not-containing
162 cholesterol. Cholesterol shifted the histograms toward higher intensities for the pT654
163 peptides (Fig. 5b, d), suggesting a cooperative effect of cholesterol and Thr
164 phosphorylation to induce higher-order assembly of the TM-JM peptides.
165
166 **Assembly of TM regions**
167 For analysis of the interactions between more than two TM or JM domains in the
168 assembled structures at the N-terminus, images of fluorescent spots containing two Cy3-
169 labeld peptides and one Cy5-labeled peptide were collected based on their 2-color
170 fluorescence trajectories (Fig. 6a). These nanodiscs showed a variety of Cy3 donor
171 fluorescence intensities before Cy5 photobleaching indicating that the three peptides
172 interacted diversely. We constructed maximum fluorescence intensity histograms in the
173 Cy3 donor channel before and after Cy5 acceptor photobleaching for inference of the
174 interactions between three TM domains (Fig. 6b–i). In all conditions other than non-
175 phosphorylated peptides in the PC/PS membrane, Cy3 distributions after Cy5
176 photobleaching (red) peaked at the fluorescence intensity of ~100 (in arbitrary units),
177 which was smaller than that observed for the C-terminal-labeled peptides (~150; Fig. 7b–
178 i). This result must have been caused by homo-FRET (self-quenching) between two N-
179 terminal labeled Cy3 peptides. Together with the very small intensity peaks prior to Cy5
180 photobleaching (blue), these distributions suggested that TM regions of the three peptides
181 (two of them were randomly labeled with Cy3) were oligomerized in very close proximity
182 to each other in the major configuration (trimer; Fig. 6j).
183 For non-phosphorylated peptides in the PC/PS membrane however (Fig. 6c), the
184 Cy3 intensity histogram after Cy5 photobleaching (red) had a peak intensity at ~150,
185 indicating that two Cy3-labeled peptides in the major population were positioned
186 separately. In addition, the low intensity shoulder in this distribution indicated the
187 presence of proximate dimers (and trimers). Taken together, these distributions suggested
188 that N-terminal regions of three non-phosphorylated peptides have a stronger tendency to
189 arrange as one dimer and one monomer in the PC/PS membrane than any other condition.
190 A similar dimer + monomer arrangement might be contained in the distributions under
191 other conditions as a minor fraction. Consistent with this suggestion, for the non-

192 phosphorylated peptides in PC/PS membrane before Cy5 photobleaching (Fig. 6c, blue),
193 a homo-FRET fraction (~100; with a low E_{FRET} to Cy5) was evident compared to other
194 conditions. It should be noted that the ability of PS to promote the dimer + monomer
195 arrangement was diminished for pT654 peptides (Fig. 6g). Cholesterol also reduced this
196 effect of PS even for non-phosphorylated peptides (Fig. 6e). As observed in the earlier
197 analysis of the TM-JM peptide dimer (Fig. 3), the effects of PS and cholesterol were
198 competitive.
199
200 **Assembly of JM regions**
201 We constructed Cy3 fluorescence intensity histograms of two Cy3 and one Cy5 peptide
202 with C-terminal-labeling in single nanodiscs in order to analyze the interactions between
203 three JM domains (Fig. 7). The distributions of the Cy3 florescence after Cy5
204 photobleaching (red) were similar under all conditions, exhibiting a single peak at ~150,
205 which was the fluorescence intensity of the two Cy3 molecules without strong
206 interactions to induce homo-FRET. Both the trimer and dimer + monomer arrangements
207 are possible if we assume that the three molecules in the trimer and two molecules in the
208 dimer are not so close that they will induce homo FRET (Fig. 7j).
209 Prior to Cy5 photobleaching (blue), the distribution peaks were observed in the
210 region of small Cy3 intensities indicating the proximity of both Cy3 molecules with Cy5
211 to induce high E_{FRET}, as observed between two molecules in a nanodisc (Fig. 4), i.e., the
212 formation of a JM trimer. An accumulation in the low intensity peak fraction was very
213 evident for non-phosphorylated peptides in the membranes containing cholesterol (Fig.
214 7d, e). On the other hand, fractions at the intensities similar to those observed after Cy5
215 photobleaching were significant for pT654 peptides in the membrane without cholesterol
216 (Fig. 7f, g). In general, pT654 peptides exhibited higher fluorescence intensity compared
217 to non-phosphorylated peptides in the corresponding membrane lipid compositions. One
218 possible explanation is that the fraction of high Cy3 intensity before Cy5 photobleaching
219 represents a Cy3 dimer in the dimer + monomer arrangement of three peptides (Fig. 7j).
220 Another possibility is that it was caused by an increased distance between three JM
221 domains in trimers, resulting from Thr phosphorylation to reduce E_{FRET} (Fig. 7j top
222 middle). These two arrangements could potentially coexist.
223 Considering the possible arrangement for the TM and JM regions of three TM-
224 JM peptides together (Figs. 6 and 7), we conclude that cholesterol induces the closely
225 proximate oligomerization of three JM domains of non-phosphorylated peptides whereas
226 PS preferentially causes a dimer + monomer arrangement, and the Thr phosphorylation
227 disrupts the JM dimer and facilitates oligomerization of peptides with separated JM

228 domains in the presence of cholesterols (Fig. 8). Because of the limitation of FRET
229 measurement, we could not distinguish whether the peptides in the oligomers directly
230 interacted or not.
231
232 **Effect of Thr phosphorylation on the Tyr phosphorylation of EGFR**
233 Our single-molecule structural analysis suggested that pT654 is a key regulator of the
234 molecular assembly of EGFR, which may affect its functions. We examined this
235 possibility in living cells. It is known that PKC activation under EGF signaling induces
236 pT654 in EGFR. This process has been thought to be a negative feedback pathway in the
237 EGFR system. We expressed a wild type (wt) or T654A mutant EGFR in CHO-K1 cells,
238 which have no intrinsic expression of EGFR. An increase in pT654 was observed for wt
239 EGFR after EGF stimulation, and treatment of these cells with phorbol-12-myristate 13-
240 acetate (PMA), a PKC activator, caused stronger phosphorylation of Thr654 regardless
241 of EGF stimulation (Fig. 9a). Application of a saturation amount (100 ng/ml) of EGF to
242 the culture medium induced phosphorylation of Tyr1068 (pY1068) of both the wt and
243 T654A mutant EGFR proteins (Fig. 9b). pY1068 is a major association site on EGFR for
244 the adaptor protein GRB2 and its levels after EGF stimulation were significantly
245 increased by the T654A mutation compared to wt, as expected from the negative effect of
246 pT654. Whereas, pretreatment with PMA decreased the pY1068 level in both the wt and
247 T654A mutant EGFR (Fig. 9c). The PMA-induced decrease in pY1068 for the wt protein
248 could be a negative effect of increased pT654, but the similar result with the T654A
249 mutant suggests that PMA has indirect effects independent of pT654.
250
251 **Single-molecule imaging of the clustering and movement of EGFR**
252 We expressed EGFR (wt and T654A) fused with GFP in CHO-K1 cells and, by using
253 single-molecule imaging, detected cluster size distributions and lateral diffusion
254 movements of EGFR molecules in the plasma membrane (Fig. 10a). Clustering of EGFR
255 was measured as the fluorescence intensity distribution of EGFR spots, and the lateral
256 diffusion movements were measured as the increase in the mean square displacement
257 (MSD) of the spots with time. Both measurements were performed before and after 10
258 min of EGF application to the medium. Application of EGF to the medium induced
259 clustering and immobilization of wt EGFR as we have reported previously(14, 27). The
260 distributions of EGFR cluster size suggest formation of oligomers containing up to more
261 than 10 molecules (Fig. 10b). The convex shapes of MSD curve with time indicate
262 subdiffusion of EGFR molecules (Fig. 10c).
263 Even in the absence of EGF, PMA treatment of cells increased fractions of

264 higher-order wt EGFR oligomers (Fig. 10b left), though diffusion movements were hardly
265 affected (Fig. 10c left). This oligomerization was not as strong as that induced by EGF in
266 the absence of PMA, and application of EGF to the PMA treated cells did not induce
267 further oligomerization at least up to 10 min but significantly decreased mobility.
268 Application of EGF induced strong oligomerization and immobilized wt EGFR in cells
269 without PMA treatment. For T654A mutant, PMA treatment hardly affected both
270 oligomerization (Fig. 10b right) and movements (Fig. 10c right) in the absence of EGF.
271 EGF induced strong oligomerization and immobilization of T654A mutant independent
272 of PMA treatment. The effect of PMA to induce EGFR oligomerization dependent on
273 Thr654 was consistent with pT654-induced oligomerization of TM-JM peptides in
274 nanodiscs.
275 In summary, single-molecule measurements suggest three states of EGFR
276 oligomerization depends on pT654 and EGF association (Fig. 10d). PMA treatment of wt
277 EGFR but not T654A mutant induced a medial level of oligomerization, which could be
278 stabilized by pT654. Strong oligomerization observed under the weak pT654 level in wt
279 EGFR and no pT654 in T654A mutant was caused by a distinct mechanism of pT654. On
280 the other hand, it is possible that immobilization of EGFR relates with its tyrosine
281 phosphorylation levels as we have observed previously (28). Immobilization in the
282 presence of PMA was more evident in T654A mutant in which pY1068 level was higher
283 than that in wt EGFR (Fig. 9), and PMA treatment decreased immobilization and pY1068
284 in wt EGFR.
285
286 **Interaction of EGFR with GRB2**
287 We finally measured the interaction of EGFR with GRB2 in living cells using a split
288 luciferase (NanoBiT) assay, in which the C-terminus of EGFR and the N-terminus of
289 GRB2 were conjugated with the large BiT (LgBiT) and the small BiT (SmBiT) of
290 NanoLuc luciferase (29), respectively. The association of EGFR and GRB2 promoted the
291 formation of active luciferase to produce chemiluminescence emission (Fig. 11a). From
292 the timecourses of the NanoBiT signal increases after EGF treatment of cells expressing
293 the wt or T654A mutant EGFR (Fig. 11b), the maximum intensities indicated a dose
294 dependent response to the EGF concentration in the medium (Fig. 11b, c). The maximum
295 intensity was significantly increased after pretreatment with PMA in cells expressing wt
296 EGFR, despite the fact that the pY1068 level was reduced after the PMA treatment (Fig.
297 9c). This effect of PMA was not observed to any extent with the T654A mutant, and the
298 GRB2 association was not increased by this mutation in the absence of PMA, even though
299 the pY1068 level after EGF stimulation was significantly increased in the mutant (Fig.

300 9c). The increase in GRB2 association observed for wt EGFR after PMA treatment was
301 not likely to be an indirect effect of PMA because it was not observed for the T654A
302 mutant, in which the pY1068 level was also affected by PMA. These results suggest that
303 pT654 promotes the formation of a GRB2 recognition state for EGFR, and that the
304 inhibition of Thr654 phosphorylation prevents a GRB2-EGFR association in spite of
305 enhanced Tyr1068 phosphorylation.
306

Discussion

We have here studied the dimerization and oligomerization of EGFR molecules by reconstituting its TM-JM peptides into nanodiscs. As expected from the positively charged JM-A sequence and accumulation of EGFR in the raft membrane, PS and cholesterol affect the molecular assembly of the TM-JM peptides. Interestingly, these two lipid species each function in a specific fashion i.e. the E_{FRET} distributions between the two TM-JM peptides in the nanodiscs suggested that PS facilitates JM dimerization, while cholesterol induces closer positioning of both the TM and JM domains (Figs. 3 and 4). In addition, cholesterol promoted the oligomeric assembly of TM-JM peptides (Figs. 6 and 7). We herein propose schematic models for the formation of the EGFR TM-JM dimers and trimers under various conditions of lipid exposure and Thr654 phosphorylation (Fig. 8), in which PS and cholesterol exert competitive effects on dimerization and oligomerization, and pT654 disrupts the PS-induced JM dimer, thus promoting oligomerization of the peptides.

It should be noted that the E_{FRET} distribution was broad in every one of our observations in this present study, especially between JM domains, indicating multiple configurations coexisting under each condition. Non-phosphorylated peptide dimers showed a peak at around $E_{FRET} > 0.90$ and > 0.81 both for N- and C-terminus labeling, respectively. We can attribute this configuration to that suggested in a previous NMR study, in which two JM domains form an anti-parallel helix dimer (9). PS stabilized this configuration probably at the JM side of the non-phosphorylated peptide. Acidic lipids are known to interact with the positively charged JM-A domain (19, 30) whereas cholesterol induced more proximation of the two peptides at the both N- and C-termini in the major configuration (E_{FRET} 0.95 and 0.93), which must be distinct from the arrangement containing antiparallel JM helices (Fig. 8). If the TM-JM domains of whole EGFR dimer adopt similar configurations as suggested for the TM-JM peptides in the nanodiscs, the arrangement of two kinase domains indicates namely, the kinase activity would be affected by the lipid composition and by pT654 (Fig. 11d).

Cholesterol was found in our current analysis to increase the population of nanodiscs containing three TM-JM peptides with pT654 (Fig. 5). The fluorescence intensity distributions of the two Cy3 probes among the three peptides in the presence of cholesterol suggested that a close trimer was the major configuration (Figs. 6 and 7). The cholesterol-induced oligomerization of TM peptides with a short JM region (to T654) of EGFR in liposomes has been reported previously from NMR analysis (31). In that report however, pT654 in the peptide showed no obvious effect on the oligomerization in PC and PC/cholesterol liposomes (without any acidic lipids), consistent with our current and

343 previous results indicating interplay of acidic lipids and pT654. The induction of
344 oligomerization seems to be a general effect of cholesterol upon α-helix peptides in lipid
345 bilayers (32). Our result does not necessarily mean trimerization in the physiological
346 conditions but reflects a tendency of oligomerization. We picked up trimers in the analysis
347 to avoid complexity in the interactions between more than three molecules. While in the
348 PC/PS membrane without cholesterol (Figs. 6 and 7), the probability to adopt a one dimer
349 + one monomer configuration seems to be increased for the non-phosphorylated peptides,
350 likely because peptides have difficulty forming trimers when containing the anti-parallel
351 helix JM dimer, the pT654 event appears to dissociate the JM dimer to help in the
352 formation of the close trimer especially in the presence of cholesterol. If this assumption
353 is correct, oligomer formation will be inhibitory for EGFR kinase activity. Our observed
354 increases in the pY1068 level in the T654A mutant of EGFR (Fig. 9) support this
355 possibility. Recently, we found that cholesterol depletion induces hyperphosphorylation
356 of Y1068 and Y1173 of EGFR upon EGF stimulation. This seems to be caused by an
357 increase in the pre-dimer fraction of EGFR. However, importantly, reactions downstream
358 of EGFR autophosphorylation, including the translocation of GRB2 to the cell surface
359 and phosphorylations of SHC, AKT, and ERK were diminished under the cholesterol
360 depletion. At the same time, clustering of EGFR over dimers was strongly inhibited (33).
361 These observations are consistent with the results of this study.
362 The antiparallel helix dimer of JM is thought to facilitate asymmetric interaction
363 between the kinase domains of EGFR, and hence its activation, in order to phosphorylate
364 tyrosine residues in the C-tail (11, 34). This tyrosine phosphorylation results in the
365 recruitment of PKC and other threonine kinases from the cytoplasm to the EGFR
366 molecules for the phosphorylation of Thr654, which is known to negatively regulate
367 EGFR signaling (26, 35). Our previous results suggested that the mechanism underlying
368 this negative effect of pT654 is the dissociation of JM dimers in the presence of acidic
369 lipids (20). At the same time, pT654 might induce the oligomerization of EGFR in the
370 presence of cholesterol. Supporting this possibility, our current single-molecule imaging
371 in living cells revealed the oligomerization of unliganded wt EGFR after PMA treatment,
372 which induced pT654 (Fig. 10). In the unliganded condition, the extracellular domains of
373 EGFR are thought to prevent the JM dimerization for kinase activation (9, 36). Clustering
374 of EGFR is also prevented largely in the unliganded condition. However, probably due to
375 the structural fluctuation, a small part of the unliganded EGFR are oligomerized (33).
376 pT654 (PMA) stabilized the unliganded oligomers possibly destructing the JM
377 antiparallel dimers.
378 We previously reported that oligomers of EGFR formed after cell stimulation

379 with EGF function as the major signal transduction sites for GRB2, where the dissociation
380 rate constant with GRB2 was reduced increasing the affinity between single-molecules
381 of EGFR and GRB2 (14). In addition, our current analyses found an increase in the wt
382 EGFR/GRB2 association following PMA treatment (Fig. 11). We speculate that after the
383 initial Tyr phosphorylation, successive Thr phosphorylation reduces Tyr kinase activity
384 of EGFR but enhances the formation of signal transduction oligomer in the medium
385 immobilized and oligomerized state of EGFR molecules (Fig. 10d). Further
386 immobilization and oligomerization were found in our current experiments to be induced
387 by EGF in the absence of PMA for wt EGFR and with or without PMA for the T654A
388 mutant. This process might include EGFR molecules accumulated into the clathrin coated
389 pits (37) and be independent of pT654. In the previous report (38), ERK activation was
390 reduced by the Thr654/669 of EGFR to Ala substitution suggesting only negative effects
391 of Thr654, however, oligomerization of EGFR was not observed in this report. Distinct
392 from wt EGFR, the T654A mutation in EGFR suppressed the GRB2 association after
393 EGF association in spite of the higher levels of Tyr phosphorylation at the binding site
394 compared to wt. Thus, even though pT654 is inhibitory for EGFR kinase activity, it
395 promotes signal transduction to the cytoplasmic protein, GRB2.
396 Based on our present results, we propose a model of EGFR signaling regulated
397 by membrane lipids and Thr654 phosphorylation (Fig. 11d). The signal transduction
398 mediated by EGFR is a complex multi-step process. Conformational changes in the
399 extracellular domain of EGFR upon ligand association allow JM domains to form acidic
400 lipid-facilitated anti-parallel JM helix dimers and asymmetric kinase domain dimers(11,
401 34). This is the activation process for EGFR kinase, in which acidic membrane lipids and
402 cholesterol play stimulative and inhibitory roles, respectively (20, 33). Tyrosine
403 phosphorylation in the kinase-active EGFR dimers recruits PKC from the cytoplasm (39).
404 The association of PLCγ to the EGFR phosphotyrosine for the degradation of PIP_2 is
405 involved in this process. PKC then phosphorylates Thr654 (40), which dissociates anti-
406 parallel JM dimers in the presence of remaining acidic lipids and supports the
407 oligomerization of EGFR in the presence of cholesterol, especially after the removal of
408 acidic lipids around the EGFR molecules. The cholesterol-induced oligomer of EGFR is
409 a major site of interaction with cytoplasmic proteins including GRB2 (14). Thus, a major
410 function of EGFR is shifted from a kinase for self-activation to a scaffold for signal
411 transduction. Thr654 phosphorylation is a key step underlying this role change of EGFR
412 and is not merely an inactivating mechanism. The degradation of PIP_2, a major anionic
413 lipid in the inner leaflet of the plasma membrane, may support this role change.
414 Importantly, both Thr654 phosphorylation and PIP_2 degradation are caused by the kinase

activation of EGFR. Hence, this represents an ingenious autoregulatory process involving membrane proteins and lipids.

418 **Materials and Methods**

419 **Materials**

420 1-palmitoyl-2-oleoyl-*sn*-phosphatidylcholine (PC), 1-palmitoyl-2-oleoyl-*sn*-
421 phosphatidylserine (PS), and cholesterol were purchased from Avanti Polar Lipids
422 (Alabaster, AL) as chloroform solutions (PC and PS) or powders (cholesterol). Cy3-
423 maleimide and Cy5-maleimide were purchased from GE Healthcare Life Sciences (Little
424 Chalfont, UK). n-octyl-b-D-glucoside (OG) was purchased from Dojindo (Kumamoto,
425 Japan). Monofunctional polyethylene glycol-succinimidyl valerate (s-PEG, 5000 mol wt)
426 and biotinylated monofunctional polyethylene glycol-succinimidyl valerate (b-PEG,
427 5000 mol wt) were purchased from Laysan Bio (Arab, AL). Chinese hamster ovary K1
428 (CHO-K1) cells were provided from RIKEN BRC through the National Bio-Resource
429 Project (MEXT, Tokyo, Japan).

430

431 **Plasmid construction**

432 Construction of the cDNA of full-length human EGFR (wt) fused with GFP was described
433 previously (14). T654A mutant DNA was constructed using PrimeSTAR Max (Takara,
434 Kusatsu, Japan) in the wt EGFR vector. The primer sequences were as follows:
435 EGFR(T654A)-f: GAAGCGCGCGCTGCGGAGGCTGCTGC and EGFR(T654A)-r:
436 CCGCAGCGCGCGCTTCCGAACGATGTG, respectively. For NanoBiT assays, full-
437 length human EGFR (wt or T654A mutant) was fused with LgBiT at the C-terminus (wt
438 or T654A EGFR-LgBiT), and GRB2 was fused with SmBiT at the N-terminus (GRB2-
439 SmBiT) as follows. The LgBiT fragment amplified from pBiT1.1-C [TK/LgBiT] Vector
440 (Promega) using KOD One PCR Master Mix (TOYOBO) was subcloned into the AgeI-
441 and NotI-digested EGFP-N1 vector (Clontech), and subsequently full-length EGFR
442 fragment was subcloned into the NheI- and HindIII-digested the LgBiT-inserted EGFP-
443 N1 vector. The GRB2-SmBiT fragment was constructed using KOD One PCR Master
444 Mix (TOYOBO) and subcloned into the AgeI- and SalI-digested EGFP-C2 vector
445 (Clontech). The primer sequence of SmBiT was designed from pBiT2.1-N [TK/SmBiT]
446 Vector (Promega).

447

448 **Peptide synthesis and purification**

449 Peptides corresponding to the TM-JM regions of EGFR (618-666) were synthesized by
450 solid-phase methods with the sequence KIPSIATGMVGALLLLLVVALGIGLFM-
451 RRRHIVRKRT$_{654}$LRRLLQERELVE-NH_2 (28). For the experiments with the C-terminal
452 labeled EGFR peptide, peptides containing a cysteine at the C-terminus were synthesized.
453 These synthetic peptides were purified by reverse-phase high-performance liquid

454 chromatography on a C4 column with a gradient of 1-propanol and acetonitrile (1:1) over
455 0.1% aqueous trifluoroacetic acid. To prepare the C-terminal labeled peptide, Cy3-
456 maleimide or Cy5-maleimide was introduced to the sulfide group on the cysteine at the
457 C-terminus of the TM-JM peptide by mixing the peptide and the fluorescence derivative
458 in dimethyl formamide under basic conditions. For experiments with the N-terminal
459 labeled peptide, Cy3-COOH or Cy5-COOH was reacted with an elongating peptide on
460 the resin in the presence of 1-[bis(dimethylamino)methylene]-1H-benzotriazolium 3-
461 oxide hexafluorophosphate (HBTU) and diisopropylethylamine (DIEA), which activate
462 the carboxyl group on the fluorophore derivative. For synthesis of Thr654 phosphorylated
463 peptides, phosphorylated threonine derivatives were utilized. The purity was confirmed
464 by reverse-phase high-performance liquid chromatography and matrix-assisted laser-
465 desorption/ionization time-of-flight mass spectroscopy analysis.
466
467 **Nanodisc preparation**
468 For nanodisc construction, fluorescent EGFR TM-JM peptides co-solubilized with lipids
469 and OG in hexafluoroisopropanol were first dried to form thin films. These peptide films
470 were then resolubilized in buffer A (0.5 M NaCl, 20 mM Tris/Cl, 0.5 mM EDTA)
471 containing 30 mM OG and 5 mM dithiothreitol (pH 7.5). His8-tagged MSP 1E3D1 (MSP)
472 was expressed in *E.* coli and purified as described previously (41). The concentration of
473 MSP was quantified based on the absorbance at 280 nm (29,910 $M^{-1}cm^{-1}$). Thin PC or PS
474 films were formed by evaporation of the solvent (chloroform) under a steam of nitrogen
475 gas and dried in vacuum. Cholesterol powders were first dissolved in chloroform, and a
476 thin film was formed as described above. PC, PS, and cholesterol were resuspended in
477 buffer A containing 0.4 M sodium cholate (pH 7.5) at a final concentration of 10 mM.
478 Cy3- and Cy5-labeled TM-JM peptides in buffer A were mixed in equal amounts and then
479 conjugated with MSP and phospholipid mixtures (PC, PC/PS, PC/cholesterol,
480 PC/PS/cholesterol) at a molar ratio of 1:1:120 μM (TM-JM/MSP/lipids). The mixture was
481 dialyzed against a buffer containing 0.5 M NaCl, 20 mM Tris/Cl, and 5 mM EDTA (pH
482 7.5) at 4°C to reconstitute the nanodiscs by removing the detergent. The aggregates and
483 liposomes were removed from the mixture by size-exclusion chromatography using a
484 Superdex 200 Increase column (GE Healthcare Life Sciences) and the peak fractions
485 containing nanodiscs of around 11 nm in diameter were collected.
486
487 **Single-pair FRET (spFRET) measurements**
488 Nanodisc samples were immobilized on the surface of a glass chamber as described
489 previously (20, 42, 43). Briefly, amine-modified glass surfaces were coated with 99% s-

PEG and 1% b-PEG. NeutrAvidin (Thermo Fisher Scientific、Waltham, MA) was then bound to the b-PEG. The nanodisc samples bound with biotinylated anti-His8-tag antibody (MBL Life Science) were loaded into the glass chamber and allowed to bind to the NeutrAvidin-coated glass surface, after which unbound nanodiscs were washed away. To reduce the photobleaching rate of Cy3 and Cy5, the nanodisc-loaded chamber was filled with dialysis buffer containing 2-mercaptoethanol at the final concentration of 0.5% (w/v). The fluorescence of Cy3 and Cy5 was observed under a TIRF microscope based on an inverted microscope (Ti2; Nikon) with a 60x oil-immersion objective (ApoTIRF 60x 1.49 NA; Nikon). The fluorescence activity of Cy3 was excited using a 532 nm laser (Compass 315M-100). Dual-color imaging was carried out through a 4x relay lens by using two EMCCD cameras (C9100-134, ImagEM; Hamamatsu Photonics, Hamamatsu, Japan) with a 200x EM gain. Images of 512 x 512 pixels (67 nm/pixel) were recorded with a temporal resolution of 100 ms/frame using MetaMorph (Molecular Devices, San Jose, CA) or AIS (ZIDO, Toyonaka, Japan).

Analysis of FRET signals

The measurement of fluorescence intensities of single nanodiscs was performed using ImageJ software, as described previously (44). The background noise was filtered out using the Subtract Background function in ImageJ. Fluorescence intensities of Cy3 and Cy5 in single nanodiscs were measured as averages from circles with a diameter of 12 pixels containing a fluorescence spot. The average intensity of the same sized circles in which no spot was present was subtracted as the background. Along the fluorescence trajectories of TM-JM-Cy3 and TM-JM-Cy5, the FRET efficiency, E_{FRET}, for each frame (> 2000) was calculated from the fluorescence intensities in the donor I_{D} and FRET I_{A} channels as

$$E_{FRET} = \frac{I_A - \beta I_D}{I_A + (\gamma - \beta) I_D},$$

where β and γ are coefficients for the compensation of fluorescence leakage from the donor dye to the acceptor detector channel, and the difference in the detection efficiencies of the dyes, respectively (45). Coefficients were calculated using the intensity time traces as $\beta = 0.03$ and $\gamma = 0.4$, respectively. E_{FRET} distributions were all different in Kolmogorov-Smirnov (KS) test with a rejection $p < 0.006$. The peak positions and their 95% percentile section were estimated using bootstrap method from a discretized E_{FRET} distribution (Table I), in which the bin width was set to 0.02 and the resampling number was 300. KS test was done using "StatsKSTest" in Igor Pro 8.0 (WaveMetrix). Resampling for

524 bootstrap method was done using “sample” function in R.
525
526 **Cell culture and transfection**
527 CHO-K1 cells were maintained in HAM F12 medium supplemented with 10% fetal
528 bovine serum at 37°C under 5% CO_2. HEK293S cells were maintained in DMEM F12
529 medium supplemented with 10% fatal bovine serum at 37°C under 5% CO2. For western
530 blotting assays, DNA constructs of full-length wt and T654A EGFR (1 μg) were
531 transiently transfected into CHO-K1 cells using FuGENE HD Transfection Reagent
532 (Promega, Madison, WI). For single-molecule measurements, CHO-K1 cells were
533 transfected with either a wt or T654A EGFR-GFP gene (0.5 μg each) using Lipofectamine
534 3000 Reagent (Thermo Fisher Scientific). For NanoBiT assays, HEK293S cells were
535 transfected with a mixture of wt or T654A EGFR-LgBiT gene (1 μg each) and GBR2-
536 SmBiT (0.2 μg) using Lipofectamine 3000 Reagent in 60 mm dish.
537
538 **PMA treatment and EGF stimulation**
539 DNA constructs of full-length wt and T654A EGFR were transfected and cultured with
540 10% fetal bovine serum (FBS) on the day before each measurement. Cells were then
541 starved in modified Eagle’s medium without FBS for 3 hours before the experiment.
542 Phorbol 12-myristate 13-acetate (PMA) was dissolved in DMSO and subsequently
543 diluted in PBS to a final concentration of 10 μM. For PMA pre-treatment, PMA solution
544 was added to the cell cultured medium at a final concentration of 100 nM and incubated
545 for 30 min at room temperature. For EGF stimulation, EGF (PeproTech, Cranbury, NJ)
546 dissolved in PBS was added to the cell cultured medium at a final concentration of 100
547 ng/mL (for western blotting assays and single-molecule measurements) or as a 0.001 to
548 100 nM dilution series (for the NanoBiT assay).
549
550 **Western blotting analysis**
551 In cells stimulated with EGF for 0, 5, 30 min at 37°C, threonine and tyrosine
552 phosphorylation of the wt and mutant T654A proteins was detected by western blotting
553 using rabbit anti-pT654 (ab75986; Abcam, Cambridge, UK) and rabbit anti-pY1086
554 antibody (#4407; Cell Signaling Technology, Danvers, MA), respectively. Rabbit anti-
555 EGFR antibody (#sc-03; Santa Cruz Biotechnology, Dallas, TX) was used to detect
556 protein expression. After being resolved by SDS-polyacrylamide gel electrophoresis
557 (PAGE), the electrophoresed proteins were transferred onto a polyvinylidene difluoride
558 (PVDF) membrane and incubated with each antibody (primary antibody) and then with a
559 horseradish peroxidase (HRP)-linked anti-rabbit IgG (secondary antibody; 7076, Cell

560 Signaling Technology). Immunoreactive proteins were detected with Amersham ECL
561 Prime Western Blotting Detection Reagent (GE Healthcare) using an ImageQuant LAS
562 500 device (GE Healthcare).
563
564 **Single-molecule imaging in living cells**
565 The methods for single-molecule measurement and analysis were described elsewhere
566 (Yanagawa and Sako, Methods in Mol Biol, in press; bioRxiv: doi:
567 10.1101/2020.06.08.141192). The single-molecule imaging of EGFR was performed at
568 the basal plasma membrane of the CHO-K1 cells at 25°C with the same microscopic
569 methods used for the spFRET measurements. The laser wavelength was 488 nm (Sapphire
570 488; Coherent, Santa Clara, CA) for the excitation of the GFP. Fluorescence images were
571 acquired every 50 ms using AIS software. The acquired multiple TIFF files were
572 processed by ImageJ software as follows: background subtraction was performed with a
573 rolling ball radius of 25 pixels, and two-frame averaging of the images was then
574 performed. Single-molecule tracking analysis was performed with AAS software (ZIDO).
575 All subsequent analyses were performed using smDynamicsAnalyzer
576 (https://github.com/masataka-yanagawa/IgorPro8-smDynamicsAnalyzer), an Igor Pro
577 8.0-based homemade program.
578
579 **NanoBiT assay**
580 HEK293S cells co-transfected with the plasmids of wt or T654A EGFR-LgBiT and
581 GRB2-SmBiT. Overnight after the transfection, cells were collected in 0.5 mM EDTA-
582 containing PBS, centrifuged, and suspended in 2 mL of HBSS containing 0.01 % bovine
583 serum albumin and 5 mM HEPES (pH 7.4) (assay buffer). The cell suspension was
584 dispensed in a 96-well white bottom plate at a volume of 80 μL per well and loaded with
585 20 μL of 25 μM Nano-Glo Vivazine Live Cell Substrates (Promega) diluted in the assay
586 buffer. After incubation for 2 hrs at room temperature in the assay buffer, cells were
587 pretreated with PMA or vehicle as described above. Basal luminescence was then
588 measured by using a microplate leader (SpectraMax L, Molecular Devices) with an
589 interval of 60 sec at room temperature. After 10 min, 20 μL of the EGF dilution series in
590 the assay buffer or the assay buffer (vehicle) were applied to each well using a benchtop
591 multi-pipetter (EDR-384SR, BioTec, Tokyo, Japan) under red dim light. Then,
592 luminescence was measured for 30 min with an interval of 60 sec. Each time-course of
593 luminescence counts was normalized with the luminescence counts of the vehicle-added
594 well. Dose-response curves were fitted with a Hill-equation to determine the maximum
595 intensity.

Acknowledgments

YS was supported by MEXT Japan with Grants-in-Aid for Scientific Research (19H05647) and by JST CREST (JPMJCR1912). We thank Hiromi Sato for technical assistance.

Author contributions

Conceptualization, R.M., Y.S.; methodology, R.M., T.S., M.Y., Y.S.; investigation, R.M., H. T., T. S., M.Y.; manuscript writing, R.M., T. S., Y.S. with feedback from all other coauthors; funding acquisition, Y.S.; supervision, Y.S.

Conflicts of interest

None.

609 **References**

610 1. M. A. Olayioye, R. M. Neve, H. A. Lane, N. E. Hynes, The ErbB signaling network:
611 receptor heterodimerization in development and cancer. *EMBO J.* **19**, 3159-3167
612 (2000).
613 2. M. K. Nyati, M. A. Morgan, F. Y. Feng, T. S. Lawrence, Integration of EGFR inhibitors
614 with radiochemotherapy. *Nat. Rev. Cancer* **6**, 876-885 (2006).
615 3. E. Kovacs, J. A. Zorn, Y. Huang, T. Barros, J. Kuriyan, A structural perspective on the
616 regulation of the epidermal growth factor receptor. *Annu. Rev. Biochem.* **84**, 739-764
617 (2015).
618 4. N. J. Bessman, M. A. Lemmon, Finding the missing links in EGFR. *Nat. Struct. Mol.*
619 *Biol.* **19**, 1-3 (2012).
620 5. H. Ogiso *et al.*, Crystal structure of the complex of human epidermal growth factor and
621 receptor extracellular domains. *Cell* **110**, 775-787 (2002).
622 6. X. Zhang, J. Gureasko, K. Shen, P. A. Cole, J. Kuriyan, An allosteric mechanism for
623 activation of the kinase domain of epidermal growth factor receptor. *Cell* **125**, 1137-
624 1149 (2006).
625 7. M. J. Wagner, M. M. Stacey, B. A. Liu, T. Pawson, Molecular mechanisms of SH2- and
626 PTB-domain-containing proteins in receptor tyrosine kinase signaling. *Cold Spring*
627 *Harb Perspect Biol* **5**, a008987 (2013).
628 8. K. M. Ferguson *et al.*, EGF activates its receptor by removing interactions that
629 autoinhibit ectodomain dimerization. *Mol. Cell* **11**, 507-517 (2003).
630 9. N. F. Endres *et al.*, Conformational coupling across the plasma membrane in activation
631 of the EGF receptor. *Cell* **152**, 543-556 (2013).
632 10. E. R. Wood *et al.*, A unique structure for epidermal growth factor receptor bound to
633 GW572016 (Lapatinib): relationships among protein conformation, inhibitor off-rate,
634 and receptor activity in tumor cells. *Cancer Res.* **64**, 6652-6659 (2004).
635 11. N. Jura *et al.*, Mechanism for activation of the EGF receptor catalytic domain by the
636 juxtamembrane segment. *Cell* **137**, 1293-1307 (2009).
637 12. S. E. Webb *et al.*, Single-molecule imaging and fluorescence lifetime imaging microscopy
638 show different structures for high- and low-affinity epidermal growth factor receptors in
639 A431 cells. *Biophys. J.* **94**, 803-819 (2008).
640 13. Y. Huang *et al.*, Molecular basis for multimerization in the activation of the epidermal
641 growth factor receptor. *Elife* **5** (2016).
642 14. M. Hiroshima *et al.*, Transient Acceleration of Epidermal Growth Factor Receptor
643 Dynamics Produces Higher-Order Signaling Clusters. *J. Mol. Biol.* **430**, 1386-1401
644 (2018).

645 15. N. Jura, Y. Shan, X. Cao, D. E. Shaw, J. Kuriyan, Structural analysis of the catalytically
646 inactive kinase domain of the human EGF receptor 3. *Proc Natl Acad Sci U S A* **106**,
647 21608-21613 (2009).
648 16. S. J. Fleishman, J. Schlessinger, N. Ben-Tal, A putative molecular-activation switch in
649 the transmembrane domain of erbB2. *Proc Natl Acad Sci U S A* **99**, 15937-15940
650 (2002).
651 17. A. Arkhipov *et al.*, Architecture and membrane interactions of the EGF receptor. *Cell*
652 **152**, 557-569 (2013).
653 18. M. Lelimousin, V. Limongelli, M. S. Sansom, Conformational Changes in the Epidermal
654 Growth Factor Receptor: Role of the Transmembrane Domain Investigated by Coarse-
655 Grained MetaDynamics Free Energy Calculations. *J. Am. Chem. Soc.* **138**, 10611-10622
656 (2016).
657 19. C. Matsushita *et al.*, Transmembrane helix orientation influences membrane binding of
658 the intracellular juxtamembrane domain in Neu receptor peptides. *Proc Natl Acad Sci U*
659 *S A* **110**, 1646-1651 (2013).
660 20. R. Maeda, T. Sato, K. Okamoto, M. Yanagawa, Y. Sako, Lipid-Protein Interplay in
661 Dimerization of Juxtamembrane Domains of Epidermal Growth Factor Receptor.
662 *Biophys. J.* **114**, 893-903 (2018).
663 21. K. B. Abd Halim, H. Koldso, M. S. P. Sansom, Interactions of the EGFR juxtamembrane
664 domain with PIP2-containing lipid bilayers: Insights from multiscale molecular dynamics
665 simulations. *Biochim Biophys Acta* **1850**, 1017-1025 (2015).
666 22. Y. Wang *et al.*, Regulation of EGFR nanocluster formation by ionic protein-lipid
667 interaction. *Cell Res.* **24**, 959-976 (2014).
668 23. Y. Liu *et al.*, The involvement of lipid rafts in epidermal growth factor-induced
669 chemotaxis of breast cancer cells. *Mol. Membr. Biol.* **24**, 91-101 (2007).
670 24. T. Furuchi, R. G. Anderson, Cholesterol depletion of caveolae causes hyperactivation of
671 extracellular signal-related kinase (ERK). *J. Biol. Chem.* **273**, 21099-21104 (1998).
672 25. T. Ringerike, F. D. Blystad, F. O. Levy, I. H. Madshus, E. Stang, Cholesterol is
673 important in control of EGF receptor kinase activity but EGF receptors are not
674 concentrated in caveolae. *J. Cell Sci.* **115**, 1331-1340 (2002).
675 26. K. A. Lund *et al.*, Phosphorylation of the Epidermal Growth-Factor Receptor at
676 Threonine 654 Inhibits Ligand-Induced Internalization and down-Regulation. *J. Biol.*
677 *Chem.* **265**, 20517-20523 (1990).
678 27. M. Hiroshima, Y. Saeki, M. Okada-Hatakeyama, Y. Sako, Dynamically varying
679 interactions between heregulin and ErbB proteins detected by single-molecule analysis
680 in living cells. *Proc Natl Acad Sci U S A* **109**, 13984-13989 (2012).

681 28. M. Yasui, M. Hiroshima, J. Kozuka, Y. Sako, M. Ueda, Automated single-molecule
682 imaging in living cells. *Nat Commun* **9**, 3061 (2018).
683 29. A. S. Dixon *et al.*, NanoLuc Complementation Reporter Optimized for Accurate
684 Measurement of Protein Interactions in Cells. *ACS Chem Biol* **11**, 400-408 (2016).
685 30. T. Sato, P. Pallavi, U. Golebiewska, S. McLaughlin, S. O. Smith, Structure of the
686 membrane reconstituted transmembrane-juxtamembrane peptide EGFR(622-660) and
687 its interaction with Ca2+/calmodulin. *Biochemistry* **45**, 12704-12714 (2006).
688 31. D. H. Jones, K. R. Barber, C. W. Grant, The EGF receptor transmembrane domain: 2H
689 NMR study of peptide phosphorylation effects in a bilayer environment. *Biochemistry*
690 **37**, 7504-7508 (1998).
691 32. K. Matsuzaki, Why and how are peptide-lipid interactions utilized for self-defense?
692 Magainins and tachyplesins as archetypes. *Biochim Biophys Acta* **1462**, 1-10 (1999).
693 33. M. Hiroshima *et al.*, Membrane cholesterol interferes with tyrosine phosphorylation but
694 facilitates the clustering and signal transduction of EGFR. *bioRxiv*
695 10.1101/2021.08.28.457965 (2021).
696 34. M. Red Brewer *et al.*, The juxtamembrane region of the EGF receptor functions as an
697 activation domain. *Mol. Cell* **34**, 641-651 (2009).
698 35. X. Li, Y. Huang, J. Jiang, S. J. Frank, ERK-dependent threonine phosphorylation of EGF
699 receptor modulates receptor downregulation and signaling. *Cell. Signal.* **20**, 2145-2155
700 (2008).
701 36. H. J. Zhu, J. Iaria, S. Orchard, F. Walker, A. W. Burgess, Epidermal growth factor
702 receptor: association of extracellular domain negatively regulates intracellular kinase
703 activation in the absence of ligand. *Growth Factors* **21**, 15-30 (2003).
704 37. L. K. Goh, F. Huang, W. Kim, S. Gygi, A. Sorkin, Multiple mechanisms collectively
705 regulate clathrin-mediated endocytosis of the epidermal growth factor receptor. *J. Cell*
706 *Biol.* **189**, 871-883 (2010).
707 38. M. Kluba, Y. Engelborghs, J. Hofkens, H. Mizuno, Inhibition of Receptor Dimerization
708 as a Novel Negative Feedback Mechanism of EGFR Signaling. *PLoS One* **10**, e0139971
709 (2015).
710 39. K. Oda, Y. Matsuoka, A. Funahashi, H. Kitano, A comprehensive pathway map of
711 epidermal growth factor receptor signaling. *Mol. Syst. Biol.* **1**, 2005 0010 (2005).
712 40. S. Aifa *et al.*, Phosphorylation of Thr654 but not Thr669 within the juxtamembrane
713 domain of the EGF receptor inhibits calmodulin binding. *Biochem. Biophys. Res.*
714 *Commun.* **347**, 381-387 (2006).
715 41. K. Kojima, Y. Imamoto, R. Maeda, T. Yamashita, Y. Shichida, Rod visual pigment
716 optimizes active state to achieve efficient G protein activation as compared with cone

717 visual pigments. *J. Biol. Chem.* **289**, 5061-5073 (2014).
718 42. M. Pirchi *et al.*, Single-molecule fluorescence spectroscopy maps the folding landscape
719 of a large protein. *Nat Commun* **2**, 493 (2011).
720 43. R. Lamichhane *et al.*, Single-molecule view of basal activity and activation mechanisms
721 of the G protein-coupled receptor β_2AR. *Proc. Natl. Acad. Sci. U. S. A.* **112**, 14254-
722 14259 (2015).
723 44. R. Maeda *et al.*, Single-molecule observation of the ligand-induced population shift of
724 rhodopsin, a G-protein-coupled receptor. *Biophys. J.* **106**, 915-924 (2014).
725 45. K. Okamoto, Y. Sako, Variational Bayes Analysis of a Photon-Based Hidden Markov
726 Model for Single-Molecule FRET Trajectories. *Biophys. J.* **103**, 1315-1324 (2012).
727

Figures

Figure 1. Construction of nanodiscs containing fluorescent TM-JM peptides of EGFR. (**a**) Amino acid sequence of the EGFR TM and JM-A domains. EX, extracellular domain; TK, tyrosine kinase domain. (**b, c**) Schematic images of nanodiscs containing dimeric TM-JM peptides fluorescently labeled at the N- (b) and C-terminus (c), respectively. (**d**) Lipid compositions used in the preparation of each nanodisc sample. The fractional ratios of PS and cholesterol mimic those in the mammalian plasma membranes. (**e**) Size-exclusion chromatography used for the purification of nanodiscs containing cholesterol (red) or not (black). The charge ratios of PC/PS/cholesterol are described in the upper table. The fraction having a peak absorbance of around 12 elution volumes (mL) was collected and used for the subsequent experiments. (**f**) A thin-layer chromatography of the nanodisc fraction containing cholesterol (fraction 12 in (**e**)). (**g**) A negative stain electron micrograph of fraction 12 in (**e**). Size distribution of the nanodiscs calculated from the images was fitted with a Gaussian function, with a mean diameter of 11 ± 2 nm.

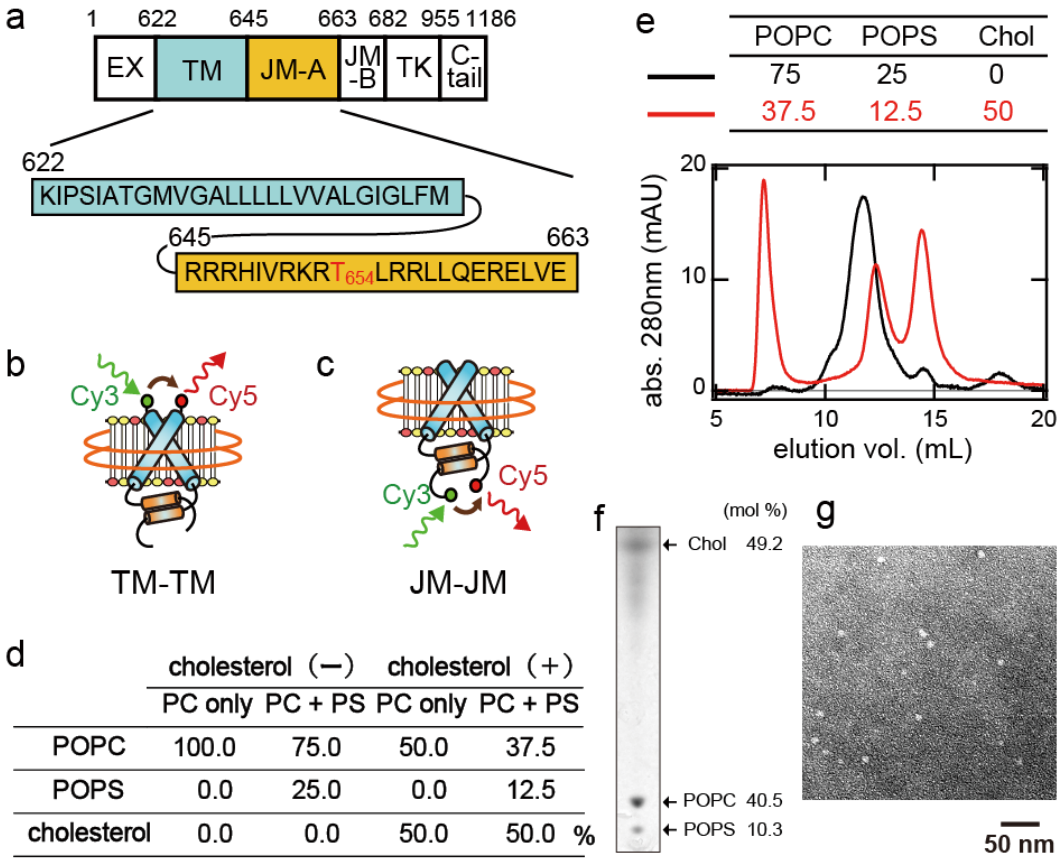

744 **Figure 2.** Single-pair FRET measurement of the EGFR TM-JM dimers in nanodiscs. (**a**)
745 Fluorescence micrograph of nanodiscs illuminated with a green laser. Cy3 (green) and
746 Cy5 (red) emissions were superimposed. The Cy5 emission was caused by FRET from
747 Cy3. (**b**) Representative fluorescence trajectories of Cy3 (green) and Cy5 (red). Black
748 allows indicate photobleaching points of Cy5. (**c**) FRET efficiency trajectories of the
749 fluorescence trajectories in **(b)**. The FRET efficiency, E_{FRET}, was calculated as described
750 in the Materials and Methods section. Typical fluorescence and FRET trajectories
751 between peptides labeled at the C-terminus are shown. Transitions to low FRET
752 efficiency states suggested that dissociation of the JM dimer occurred occasionally. The
753 Förster radius R_0 between Cy3 and Cy5 is 5.6 nm.
754

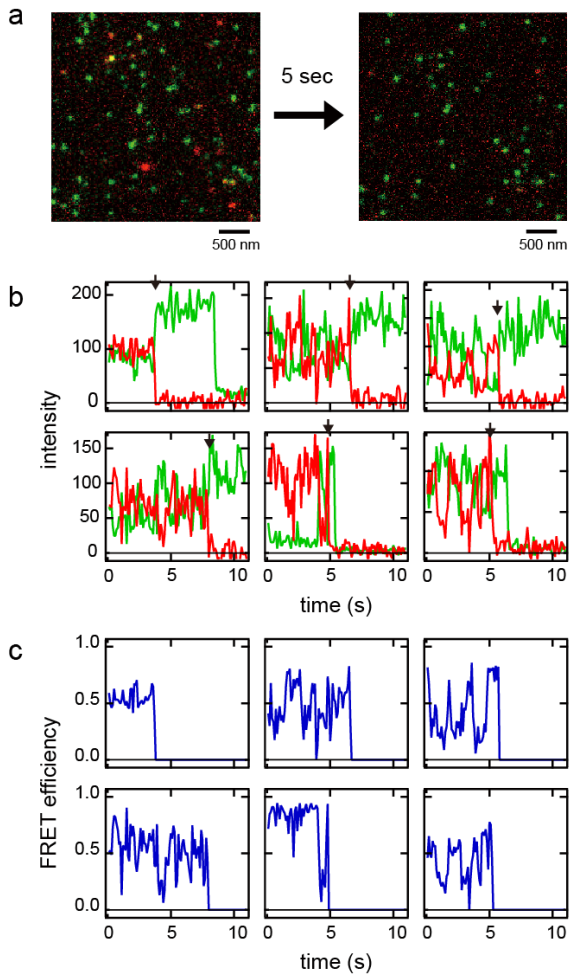

755
756

Figure 3. FRET efficiency (E_{FRET}) distributions in nanodiscs containing a single Cy3/Cy5-pair of N-terminal labeled peptides. Nanodiscs contained non-phosphorylated (**a–d**) and Thr654 phosphorylated (**e–h**) peptides at the indicated lipid conditions. Positions of the mode and its 5-95% percentile section are indicated by solid and dashed lines, respectively. See Table I for these values. In **(b–h)**, the distribution and the 95% percentile section shown in **(a)** are superimposed (red) for comparison.

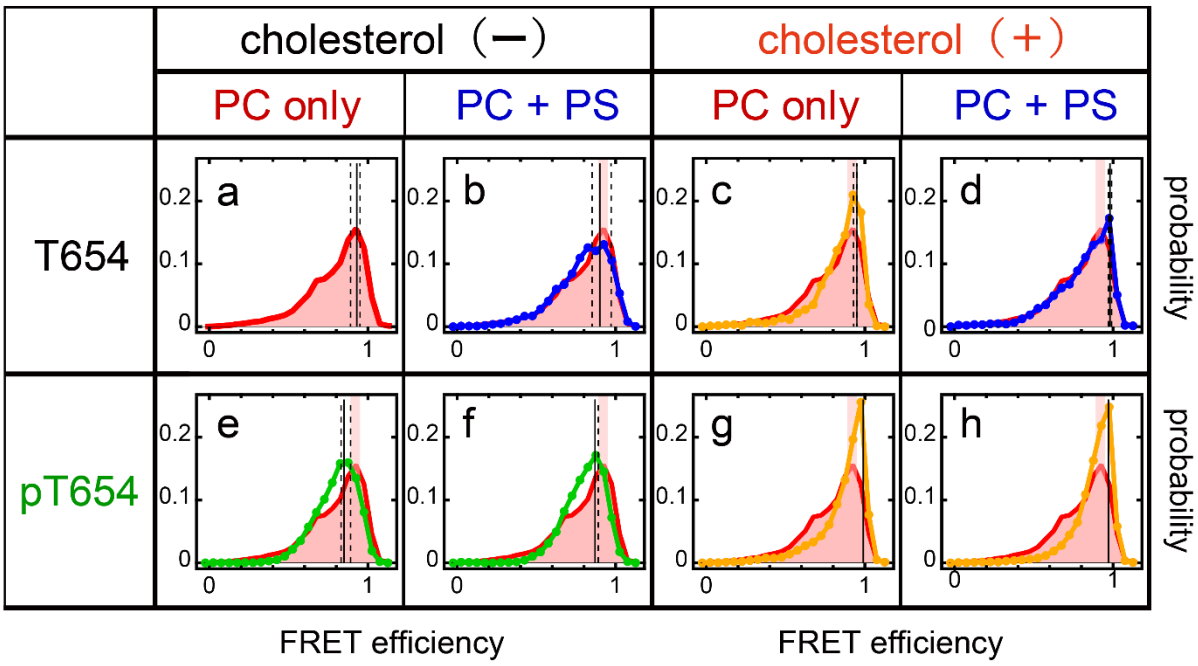

Figure 4. E_{FRET} distributions in nanodiscs containing a single Cy3/Cy5-pair of C-terminal labeled peptides. Nanodiscs contained non-phosphorylated (**a–d**) and Thr654 phosphorylated (**e–h**) peptides in the indicated lipid conditions. Positions of the mode and its 5-95% percentile section are indicated by solid and dashed lines, respectively. See Table I for these values. In **(b–h)**, the distribution and the 95% percentile section shown in **(a)** are superimposed (red) for comparison.

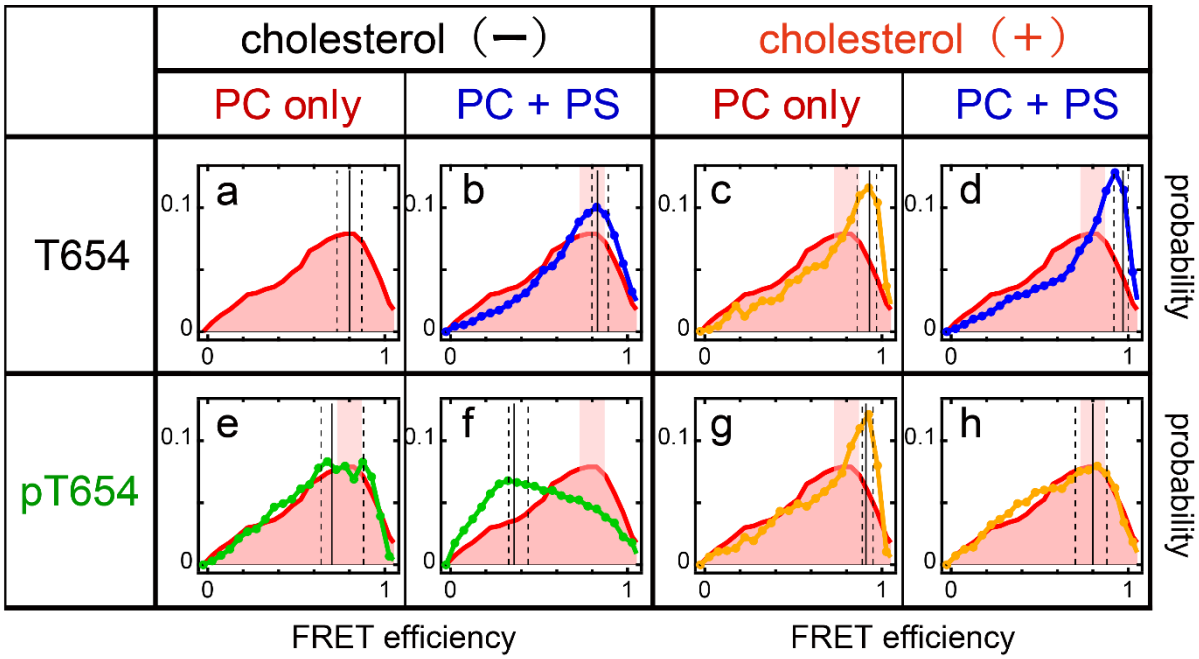

Figure 5. Higher-order oligomerization of EGFR TM-JM peptides in the nanodiscs. Histograms are shown of the total fluorescence intensity of the peptides with Cy3-labeling at the C-terminus in single nanodiscs containing cholesterol (blue) or not (red). Discs containing no Cy5 peptide were chosen for measurement to avoid the possible effects of FRET. Peptides with a non-phosphorylated **(a, c)** or phosphorylated **(b, d)** Thr654 were reconstituted into nanodiscs in PC **(a, b)** or PC/PS **(c, d)** membranes.

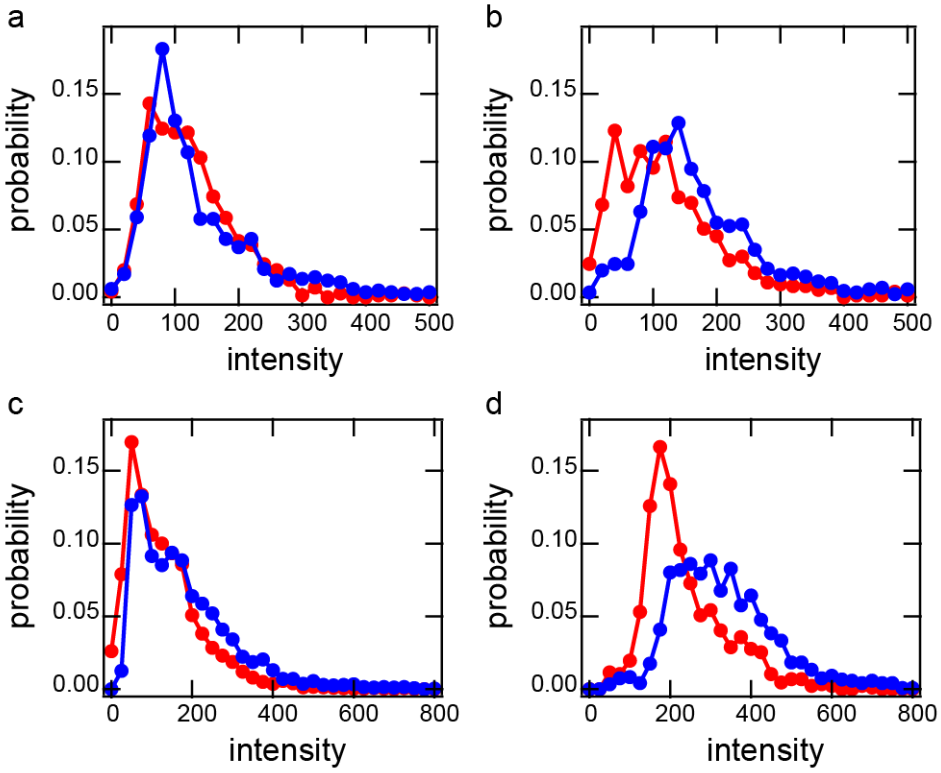

Figure 6. Assembly of EGFR TM regions. (**a**) Representative fluorescence trajectories of Cy3 (green) and Cy5 (red) in nanodiscs containing two Cy3-labeled and one Cy5-labeled peptide. Fluorescence intensities and/or two-step photobleaching dynamics after Cy5 photobleaching indicated that these nanodiscs contained two Cy3 peptides. (**b–i**) Fluorescence intensity histograms of N-terminal-labeled Cy3 peptides before (blue) and after (red) Cy5 photobleaching. Nanodiscs contained non-phosphorylated **(b–e)** and Thr654 phosphorylated **(f–i)** peptides at the indicated lipid conditions. (**j**) Schematic structures indicating proximity between three TM domains before (left) and after (right) Cy5 photobleaching. Note that acceptance of the excitation energy from Cy3 was not saturated for Cy5 under our experimental conditions, even in the presence of two Cy3 molecules.

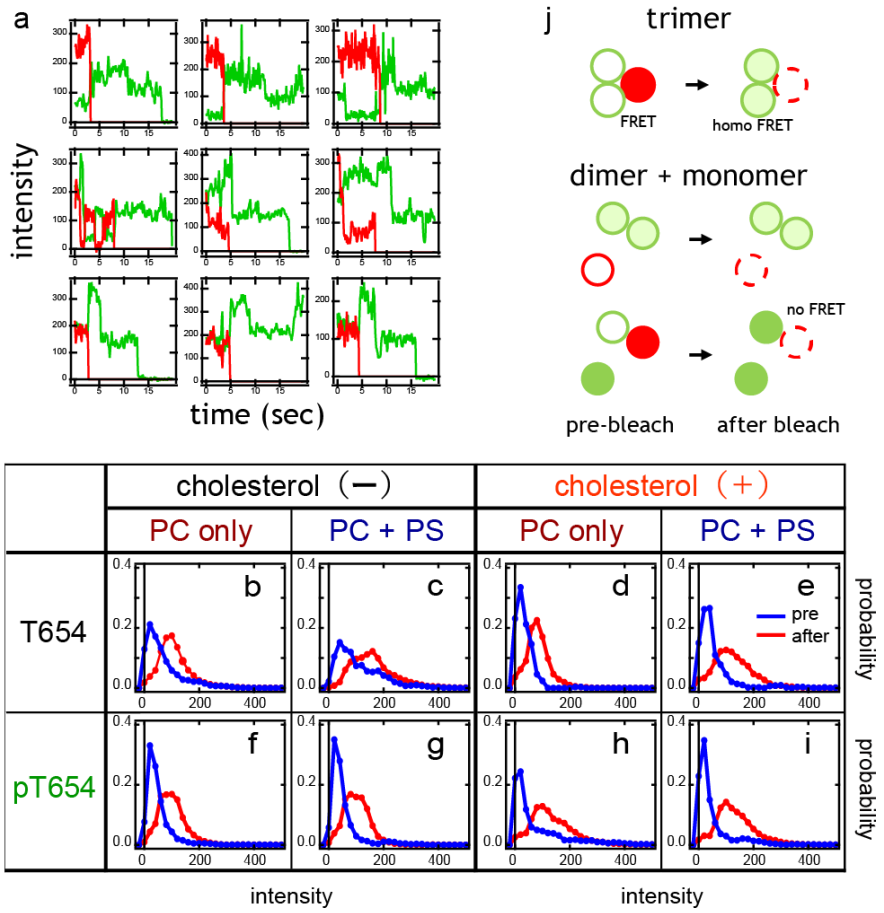

Figure 7. Assembly of EGFR JM regions. (**a**) Representative fluorescence trajectories of Cy3 (green) and Cy5 (red) in nanodiscs containing two Cy3-labeled and one Cy5-labeled peptide at the C-terminus. (**b–i**) Fluorescence intensity histograms of C-terminal-labeled Cy3 peptides from nanodiscs containing two Cy3 and one Cy5 peptide before (blue) and after (red) Cy5 photobleaching. Nanodiscs contained non-phosphorylated **(b–e)** and Thr654 phosphorylated **(f–i)** peptides at the indicated lipid conditions. (**j**) Schematic structures indicating proximity between three JM domains before (left and middle) and after (right) Cy5 photobleaching.

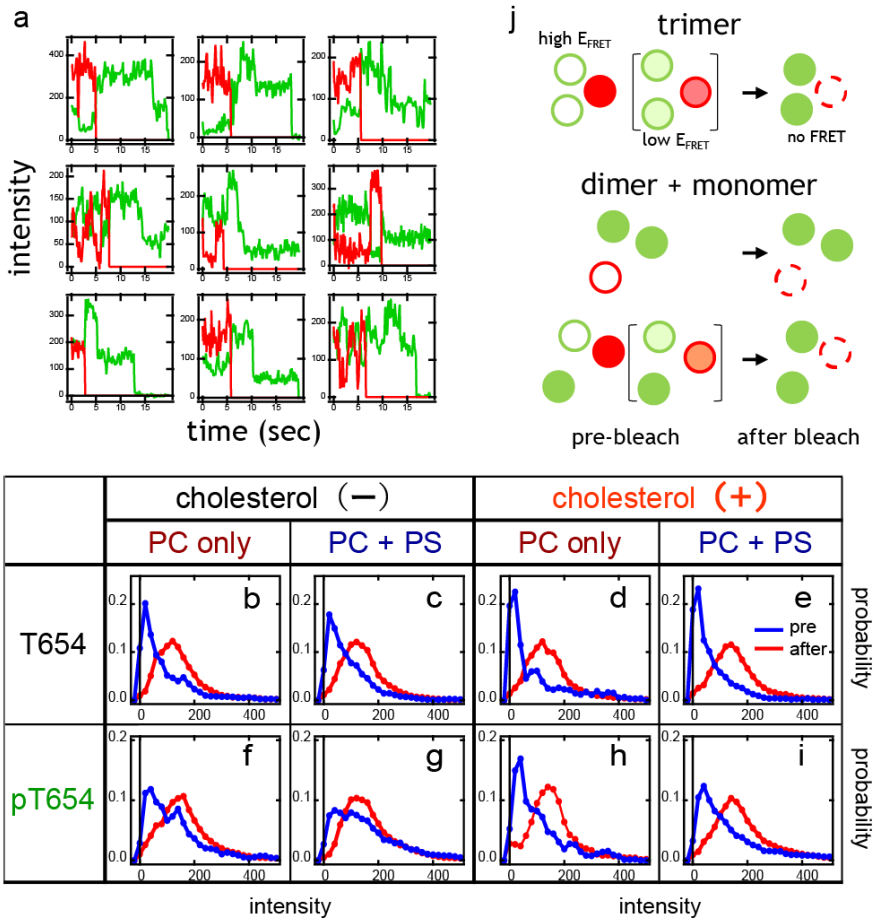

808 **Figure 8.** Possible configurations of EGFR TM-JM dimers and trimers regulated by
809 membrane lipids and Thr654 phosphorylation.
810

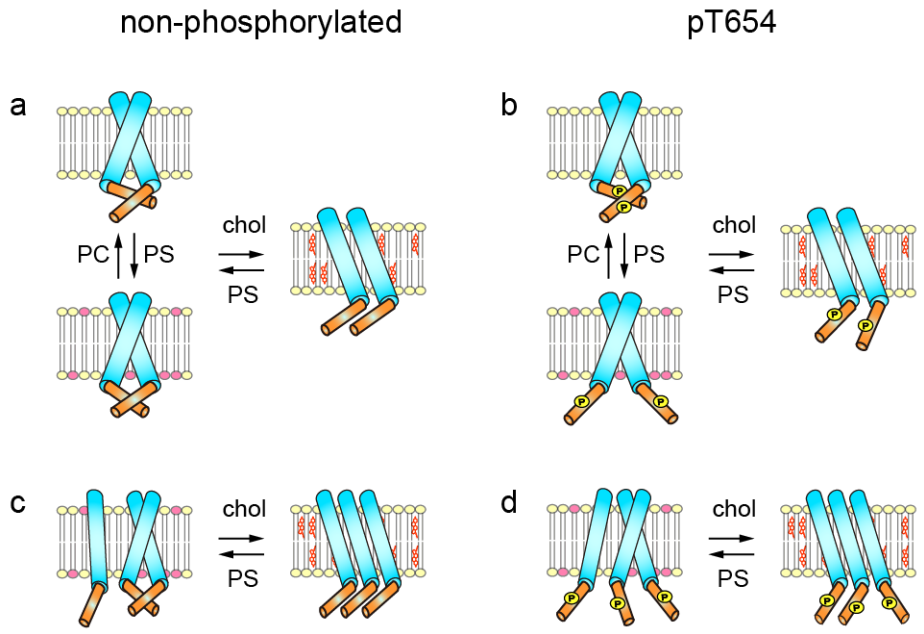

811

Figure 9. Thr and Tyr phosphorylation of EGFR. (**a**) Thr654 phosphorylation after EGF stimulation and PMA pretreatment. (**b, c**) Timecourses of Y1068 phosphorylation for the wt and T654A mutant of EGFR during EGF stimulation. Typical western blotting results are indicated **(b, top)** and the average of four independent experiments are shown with SE **(c)**. Phosphorylation levels were normalized to the expression levels of the whole EGFR molecule **(b, bottom)**.

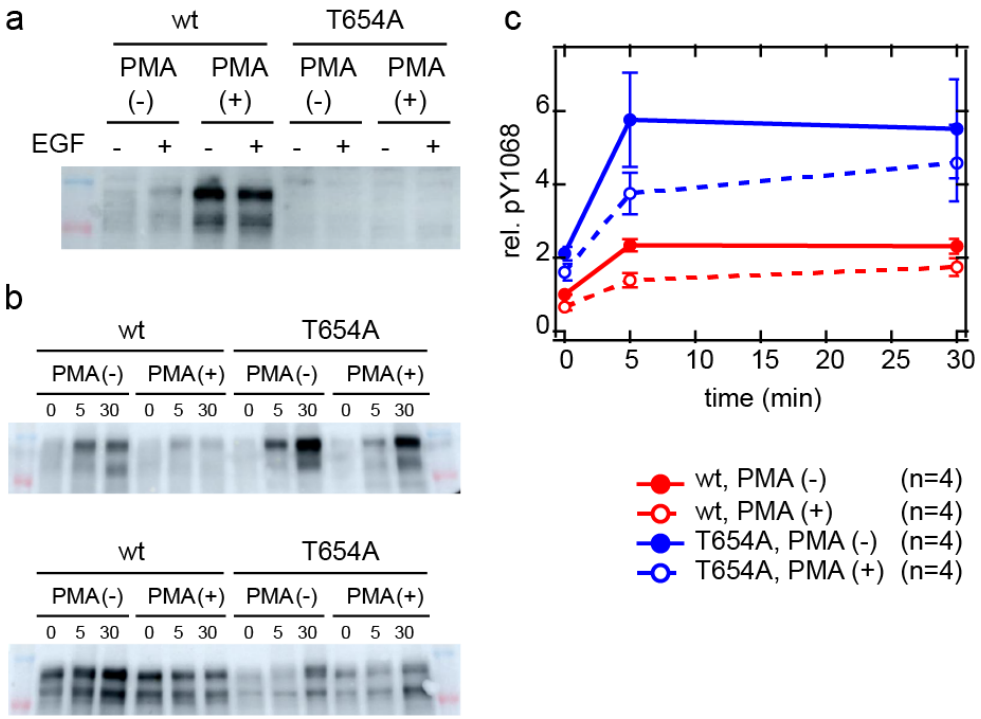

Figure 10. Oligomerization and lateral movements of EGFR on the living cell surface. (**a**) Single molecule imaging of wt EGFR-GFP on the surface of living CHO-K1 cells with (right) and without (left) PMA pretreatment. Cells were stimulated with (lower) and without (upper) EGF. Bar, 5 μm. Quantized transitions in the fluorescence intensities (bottom) indicate a single-molecule resolution of the imaging. (**b**) Oligomer size distributions of wt (left) and T654A mutant (right) EGFR in cells. The oligomer size ratio was measured before and 10 min after EGF stimulation. (**c**) Mean square displacement (MSD) of wt (left) and T654A (right) EGFR spots as a function of the time interval, indicating lateral mobility. The MSD was calculated before and 10 min after EGF stimulation. In **(b, c)**, cells were pretreated with (blue, green) or without (black, red) PMA and stimulated (red, green) or not (black, blue) with EGF. (**d**) Diagram of the oligomerization and immobilization states of wt (left) and T654A mutant (right) EGFR suggested from single-molecule measurements. Arrows indicate the state transitions after PMA treatment and EGF stimulation.

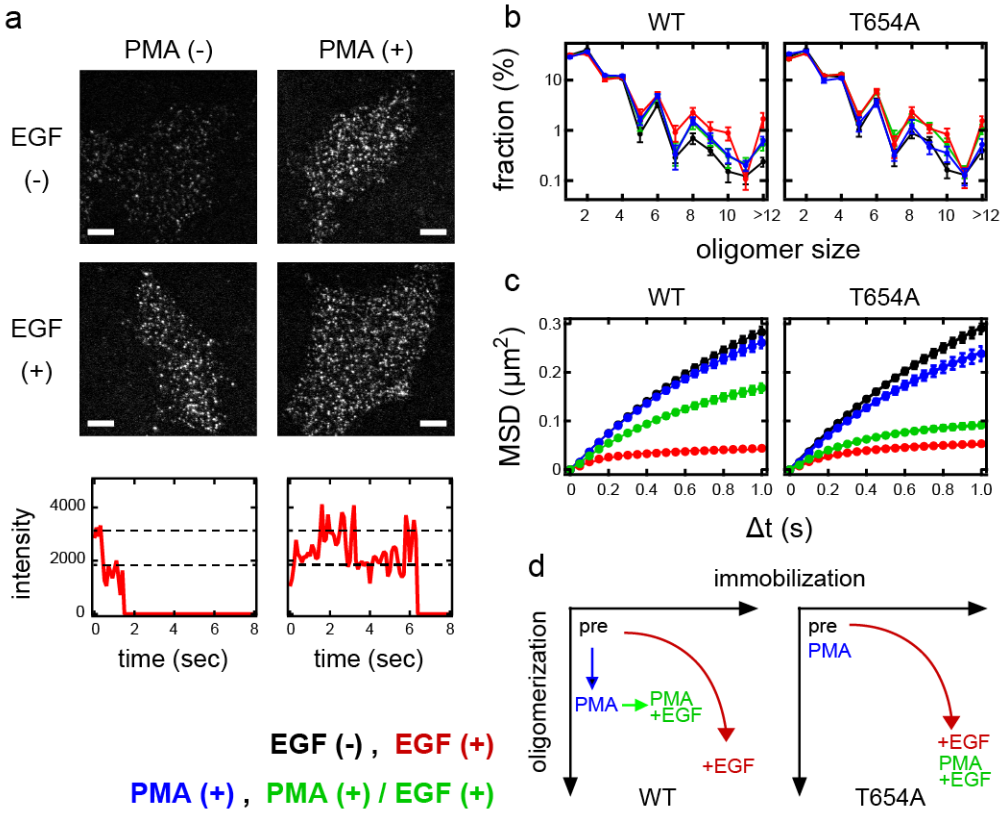

838 **Figure 11.** NanoBiT assay for the EGFR/GRB2 interaction in living cells. (**a**) Schematic
839 illustration of the NanoBiT assay of EGFR/GRB2 interactions. (**b**) Typical time courses
840 of chemiluminescence signals generated from the complex formation of large BiT
841 (LgBiT)-fused EGFR and small BiT (SmBiT)-fused GRB2 after EGF application at time
842 0. The final concentration of EGF in the culture medium was varied from 0.0001 to 100
843 nM. Measurements were done in cells with (+) or without (-) PMA pretreatment. (**c**) Dose
844 dependency of the chemiluminescence intensities at 30 min after EGF stimulation. The
845 average values from four independent experiments are shown with SE. Lines indicate
846 fitting with a Hill-equation function. *$p < 0.05$ determined by *t*-test against the signal in
847 wt cells without PMA. (**d**) A schematic model of the activation and signal transduction
848 process for EGFR dimers and oligomers. In the oligomers of EGFR, affinity with GRB_2
849 is increased.
850

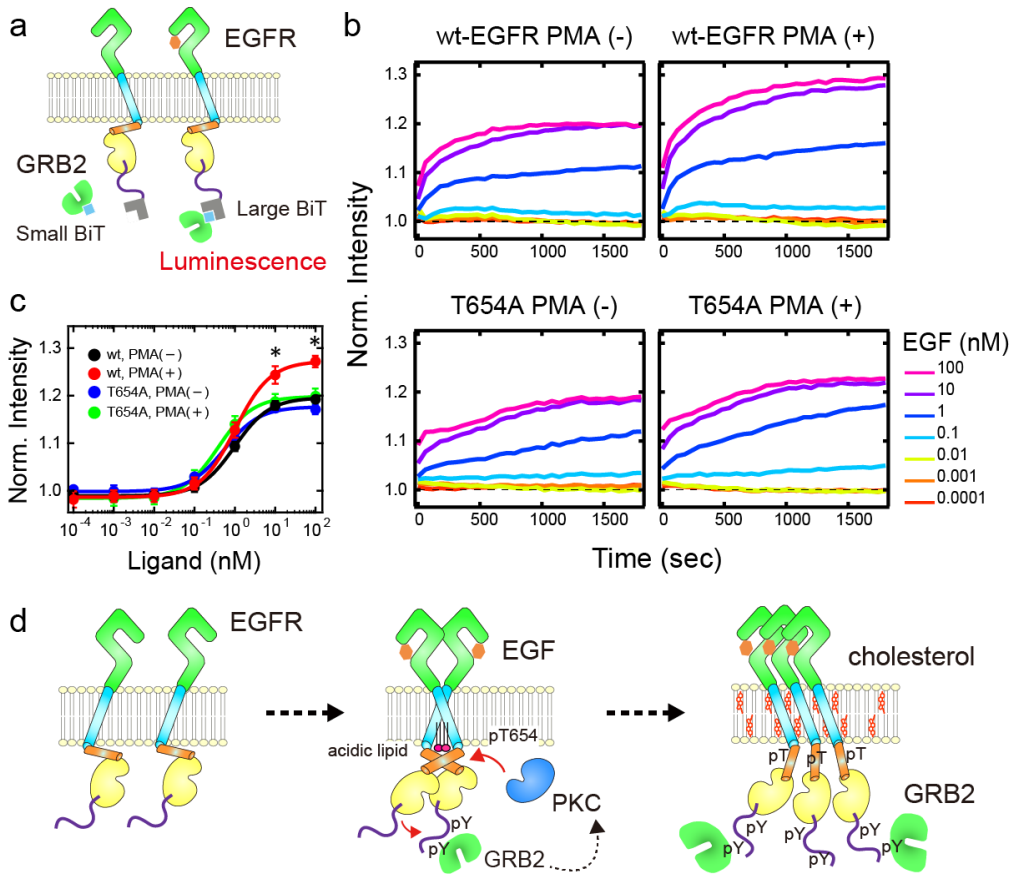

851

852 **Table I. Peak values in the E_{FRET} distributions between the TM-JM peptides**

853

lipid composition	pT654	labelling			
		N-term		C-term	
		mean	95%	mean	95%
PC	-	0.93	(0.89-0.95)	0.81	(0.73-0.87)
PC/PS	-	0.90	(0.85-0.97)	0.83	(0.79-0.89)
PC/chol	-	0.95	(0.93-0.95)	0.93	(0.85-0.97)
PC/PS/chol	-	0.98	(0.97-0.99)	0.94	(0.91-0.97)
PC	+	0.85	(0.83-0.89)	0.68	(0.63-0.89)
PC/PS	+	0.87	(0.87-0.89)	0.36	(0.33-0.43)
PC/chol	+	0.99	(0.99)	0.90	(0.89-0.95)
PC/PS/chol	+	0.97	(0.97)	0.82	(0.81-0.89)

854

855

856 Mean and their 95% percentile section of the peak values in Figs 3 and 4 were estimated
857 by bootstrap method with 300-times of resampling. An increase of the resampling times
858 to 1000 did not change the result.